APPLICATION OF AN UNSTEADY TWO-EQUATION TURBULENCE MODEL TO THE NUMERICAL PREDICTION OF THE TRANSONIC BUFFET OF AN AIRFOIL

R. Arina[1], N. Ceresola[2] and P.G. Piantà[3]

[1] Aerospace Eng. Dept. - Politecnico di Torino, Torino, Italy
[2] ALENIA - Engineering Area Aeronautica, Torino, Italy
[3] CSDF - Consiglio Nazionale delle Ricerche, Torino, Italy

Abstract. A two-equation $k - \mathcal{R}$ turbulence model, with pointwise formulation, is applied to the solution of the phase averaged Navier-Stokes equations for the simulation of shock-induced flow oscillations over a 18-percent thick circular-arc airfoil. The governing equations are solved with an implicit time discretization, with pseudo-time subiterations. The numerical computations show that the unsteady separated flow is properly predicted and better calculated than previous simulations obtained using algebraic turbulence models. The reduced frequency of oscillations is predicted 10-percent lower than the experimental one. The surface pressure distribution is in agreement with previous calculation performed with a one-equation turbulence model.

Introduction

The solution of the averaged Navier-Stokes equations for the numerical simulation of unsteady turbulent flows is currently of great interest for industrial applications. However the results are not completely satisfactory yet. While efficient and time accurate numerical techniques have been devised [1], the current turbulence models are not well-suited for unsteady flows.

Inhomogeneous turbulence, characterized by processes of energy transport and energy transfer by pressure fluctuations, such as in turbulent unsteady flows, does not have an universal eddy structure. The eddies can have distinct types of dynamical forms. We may have *vortical* eddies, which are local regions of high vorticity that may be advected by the flow, and on interacting with each other may merge and split into smaller scale motions. When moving across a mean shear flow they induce Reynolds stresses. Alternatively we may have *structural* eddies displaying a relatively fixed pattern and location within a turbulent flow. These two distinct forms of eddy structure are particularly noticeable in direct numerical simulations of turbulent boundary layers, showing that structural eddies are located near the wall, and vortical eddies are present in the outer part. In shear flows, the large scale vortical eddies are determined by the initial and boundary conditions, the mean profile and how the flow evolves.

The presence of vortical and structural vortices implies the existence of different length scales. The presence of eddy motions with different ranges of length scales is reflected in the location of the maximum of the energy spectrum. The vortical (large) eddies are located in the region of small wavenumbers, while the smaller structural eddies correspond to higher wavenumbers. In the unsteady case, the flow evolution is such that the vortical eddies are usually located in a narrow band, therefore the energy spectrum will present the maximum located at relatively small wavenumbers. In such a situation, the more elementar one-point closure models are not fully satisfactory, because they rely on a energy spectrum form which corresponds more to flows that are essentially perturbations of shear flows.

One possibility to overcome these difficulties is to devise ad hoc simple unsteady models based on algebraic or one-equation steady models for specific application. A more fruitful approach, but more expensive, is to employ a turbulence model based on two transport equations, such as the $k-\varepsilon$ model or similar models.

The objective of the present work is to devise a prediction method for unsteady compressible turbulent flows, based on the averaged Navier-Stokes equations and a two-equation turbulence model. In the next Section, we describe the more appropriate averaging process for the Navier-Stokes equations leading to a natural splitting of the contribution of the large and small scales to the turbulent stresses. Then we apply the two-equation turbulence model to the simulation of a 18-percent thick circular-arc airfoil under flow conditions for which

self-excited shock-induced oscillations occur [2].

Phase-Averaged Navier-Stokes Equations

In unsteady flows with a well defined forcing mechanism, such as vortex shedding or pressure fluctuations, organized large eddies are present. The operation of Reynolds averaging in the equation of motion hides many important features of such turbulent flows. A more appropriate flow decomposition can be obtained by viewing any fluctuating flow variable $f(\mathrm{x},t)$ as, following [3],

$$f(\mathrm{x},t) = \overline{f}(\mathrm{x},t) + \overline{\overline{f}}(\mathrm{x},t) + f'(\mathrm{x},t) \quad , \qquad (1)$$

with $\overline{f}(\mathrm{x},t)$ a global mean component defined as the time-averaged contribution; $\overline{\overline{f}}(\mathrm{x},t)$ the periodic mean component, and $f'(\mathrm{x},t)$ the random component. Defining the phase average, obtained as average over a large ensemble of N points at constant phase, as

$$< f(\mathrm{x},t) >= lim_{N\to\infty} \sum_{n=0}^{N} f(\mathrm{x},t+n\tau) \quad ,$$

the periodic wave component $\overline{\overline{f}}$ is defined as

$$\overline{\overline{f}} =< f > -\overline{f} \quad . \qquad (2)$$

Therefore the phase-averaging process eliminates the random fluctuations due to the small scale motion, and extracts only the large coherent motion from the total signal. Between the properties that follow from the above definitions, reported in [3] and [4], we have that $< f' >= 0$, the random fluctuations have zero mean at constant phase, and $\overline{\overline{f}f'} = 0$, the large scale fluctuations and the random fluctuations are uncorrelated. From relations (1) and (2), it follows

$$f =< f > +f' \quad . \qquad (3)$$

The above decomposition can be introduced into the Navier-Stokes equations and derive the equations for the global mean component, obtained inserting decomposition (1) into the Navier-Stokes equations, phase averaging and then time averaging. Being interested into compressible flows, the time averaging is replaced by the Favre averaging, and decomposition (1) is replaced by

$$f(\mathrm{x},t) = \tilde{f}(\mathrm{x},t) + \overline{\overline{f}}(\mathrm{x},t) + f''(\mathrm{x},t) \quad , \qquad (4)$$

with $\tilde{f} = \overline{\rho f}/\overline{\rho}$, and f'' are the random fluctuations. The governing equations for the Favre averaged quantities are, in nondimensional form

$$\frac{\partial \overline{\rho}}{\partial t} + \frac{\partial}{\partial x_i}(\overline{\rho}\tilde{u}_i) = 0 \quad , \qquad (5)$$

$$\frac{\partial}{\partial t}(\overline{\rho}\tilde{u}_i) + \frac{\partial}{\partial x_j}(\overline{\rho}\tilde{u}_i\tilde{u}_j + \overline{p}\delta_{ij}) = \qquad (6)$$
$$\frac{1}{Re}\frac{\partial}{\partial x_j}\left(\overline{\mu}\frac{\partial \tilde{u}_i}{\partial x_j}\right) - \frac{\partial}{\partial x_j}\left(\overline{\rho}\,\widetilde{u_i''u_j''} + \overline{\rho}\,\widetilde{\overline{\overline{u}}_i\overline{\overline{u}}_j}\right) \quad ,$$

$$\frac{\partial}{\partial t}(\overline{\rho}\tilde{E}) + \frac{\partial}{\partial x_i}\left[(\overline{\rho}\tilde{E} + \overline{p})\tilde{u}_i\right] = \qquad (7)$$
$$\frac{1}{Re}\frac{\partial}{\partial x_i}\left(\overline{\mu}\tilde{u}_j\frac{\partial \tilde{u}_i}{\partial x_j}\right) - \frac{\partial}{\partial x_i}\left[\left(\overline{\rho}\widetilde{u_i''u_j''} + \overline{\rho}\,\widetilde{\overline{\overline{u}}_i\overline{\overline{u}}_j}\right)\tilde{u}_j\right]$$
$$+\frac{1}{Re}\frac{\partial}{\partial x_i}\left(\frac{1}{\gamma-1}\frac{\overline{\mu}}{Pr}\frac{\partial \tilde{T}}{\partial x_i}\right)$$
$$-\frac{\partial}{\partial x_i}\left(\overline{\rho}\widetilde{u_i''T''} + \overline{\rho}\,\widetilde{\overline{\overline{u}}_i\overline{\overline{T}}}\right) \quad .$$

Being $\overline{\rho}$ the density, $\overline{p}$ the pressure, $\tilde{T}$ the temperature, $\tilde{E} = \tilde{\mathrm{e}} + \tilde{u}_i\tilde{u}_i/2 + k$ the total energy, $\tilde{\mathrm{e}}$ the internal energy, $\tilde{u}_i$ the velocity components, k the total kinetic energy associated with the velocity fluctuations u_i'' and $\overline{\overline{u}}_i$. The dynamic viscosity $\overline{\mu}$ is related to the temperature by the Sutherland law. Re is the reference Reynolds number. The gas is assumed perfect (air, $\gamma = 1.4$, $Pr = 0.72$).

As pointed out in [5], any averaging process, which commutes with spatial and temporal derivatives, leads to averaged equations of the same form as the Reynolds equations. Equations (5), (6) and (7) have the additional property of displaying explicitly the contribution of the small scale and large scale motion to the Reynolds stresses and the turbulent heat flux, associated with the Favre averaged global mean flow.

Two-Equation Turbulence Model

The Reynolds stresses, appearing in the averaged equations (5), (6) and (7), are related to the mean deformation tensor

$$\tilde{S}_{ij} = \frac{1}{2}\left(\frac{\partial \tilde{u}_i}{\partial x_j} + \frac{\partial \tilde{u}_j}{\partial x_i}\right) \quad ,$$

by the Boussinesq hyphotesis as follows

$$R_{ij} = -\overline{\rho}\,\widetilde{\overline{\overline{u}}_i\overline{\overline{u}}_j} - \overline{\rho}\,\widetilde{u_i''u_j''} \qquad (8)$$
$$= 2\mu_t\left(\tilde{S}_{ij} - \frac{1}{3}\delta_{ij}\frac{\partial \tilde{u}_k}{\partial x_k}\right) - \frac{2}{3}\overline{\rho}k\delta_{ij} \quad ,$$

Similarly the turbulence heat fluxes are related to the mean temperature gradient as follows, Pr_t being the turbulent Prandtl number,

$$(q_t)_i = -\overline{\rho}\,\widetilde{\overline{u}_i\overline{T}} - \overline{\rho}\,\widetilde{u_i''T''} \qquad (9)$$
$$= \frac{1}{\gamma-1}\frac{\mu_t}{Pr_t}\frac{\partial\tilde{T}}{\partial x_i} \quad .$$

The eddy viscosity is evaluated as

$$\mu_t = C_\mu\overline{\rho}\frac{k^2}{\varepsilon} \quad , \qquad (10)$$

where k is the turbulence kinetic energy and ε the dissipation rate.

The transport equations for the kinetic energy and the dissipation rate, written in nondimensional form as

$$\frac{\partial}{\partial t}(\overline{\rho}k) + \frac{\partial}{\partial x_i}(\overline{\rho}\tilde{u}_i k) = \qquad (11)$$
$$\frac{1}{Re}\mathcal{P} - \overline{\rho}\varepsilon$$
$$+\frac{1}{Re}\frac{\partial}{\partial x_i}\left[\left(\overline{\mu}+\frac{\mu_t}{\sigma_k}\right)\frac{\partial k}{\partial x_i}\right] \quad ,$$

$$\frac{\partial}{\partial t}(\overline{\rho}\varepsilon) + \frac{\partial}{\partial x_i}(\overline{\rho}\tilde{u}_i\varepsilon) = \qquad (12)$$
$$\frac{1}{Re}C_{\varepsilon 1}f_1\frac{\varepsilon}{k}\mathcal{P} - C_{\varepsilon 2}f_2\overline{\rho}\frac{\varepsilon^2}{k} +$$
$$\frac{1}{Re}\frac{\partial}{\partial x_i}\left[\left(\overline{\mu}+\frac{\mu_t}{\sigma_\varepsilon}\right)\frac{\partial\varepsilon}{\partial x_i}\right] \quad ,$$

form the standard low-Re $k-\varepsilon$ model [6].

$$\mathcal{P} = R_{ij}\frac{\partial\tilde{u}_i}{\partial x_j} \quad ,$$

is the production term. The low-Re damping effects are taken into account by the near-wall functions f_1 and f_2, as well as by the function f_μ in the low-Re expression of the eddy viscosity (10)

$$\mu_t = f_\mu C_\mu\overline{\rho}\frac{k^2}{\varepsilon} \quad . \qquad (13)$$

Usually the near-wall functions require the explicit evaluation of the distance from the wall [7]. This evaluation may be cumbersome when multiple shear layers and regions with separated flow are present. Moreover the solution of the $k-\varepsilon$ equations (11) and (12) implies numerical difficulties. To avoid both difficulties, the basic $k-\varepsilon$ equations are rewritten transforming the basic variables. Following [8], we introduce as new variable the turbulent Reynolds number

$$R_T = \frac{\overline{\rho}k^2}{\overline{\mu}\varepsilon} \quad .$$

A transport equation for the variable $\mathcal{R} = \overline{\mu}R_T/\overline{\rho}$ may be obtained from equations (11) and (12). The $k-\mathcal{R}$ low-Re model reads

$$\frac{\partial}{\partial t}(\overline{\rho}k) + \frac{\partial}{\partial x_i}(\overline{\rho}\tilde{u}_i k) = \qquad (14)$$
$$\frac{1}{Re}\mathcal{P} - \frac{\overline{\rho}k^2}{\mathcal{R}}$$
$$+\frac{1}{Re}\frac{\partial}{\partial x_i}\left[\left(\overline{\mu}+\frac{\mu_t}{\sigma_k}\right)\frac{\partial k}{\partial x_i}\right] \quad ,$$

$$\frac{\partial\mathcal{R}}{\partial t} + \frac{\partial}{\partial x_i}(\tilde{u}_i\mathcal{R}) = \qquad (15)$$
$$\frac{1}{Re}(2-C_{\varepsilon 1}f_1)\frac{\mathcal{R}}{\overline{\rho}k}\mathcal{P} - (2-C_{\varepsilon 2}f_2)\,k +$$
$$\frac{1}{Re}\frac{1}{\rho}\left(\overline{\mu}+\frac{\mu_t}{\sigma_\varepsilon}\right)\frac{\partial^2\mathcal{R}}{\partial x_i^2} - \frac{1}{Re}\frac{1}{\sigma_\varepsilon}\frac{\partial}{\partial x_i}\left(\frac{\mu_t}{\overline{\rho}}\right)\frac{\partial\mathcal{R}}{\partial x_i} \quad .$$

With the above assumptions, the eddy viscosity relation (13) can be rewritten in the form

$$\mu_t = f_\mu C_\mu\overline{\rho}\mathcal{R} \quad .$$

The model constants are

$$C_\mu = 0.09 \quad ,$$

$$C_{\varepsilon 1} = 1.44 \quad , \quad C_{\varepsilon 2} = 1.92 \quad ,$$

$$\sigma_k = 1.0 \quad , \quad \sigma_\varepsilon = \frac{(C_{\varepsilon 2}-C_{\varepsilon 1})\sqrt{C_\mu}}{\kappa^2} \quad ,$$

with $\kappa = 0.41$ the Von Kármán constant. To obtain a pointwise formulation of the turbulence model, the near-wall functions are expressed in terms of R_T, as in [6] and [7],

$$f_1 = 1 \quad ,$$

$$f_2 = 1 - 0.22e^{-\left(\frac{R_T}{6}\right)^2} \quad ,$$

$$f_\mu = e^{-\frac{3.4}{(1+R_T/50)^2}} \quad .$$

The supercritical flow about a 18-percent-thick circular-arc airfoil has been extensively investigated in the past years both experimentally [2],[9],[10], and numerically [2],[11],[12],[1]. For a test Mach number $M_\infty = 0.76$ and a chord-based Reynolds number of 11×10^6, the supercritical flow is unsteady, with self-excited shock-induced flow oscillations occurring on the upper and lower surface of the airfoil, alternately 180 deg. out of phase.

On the upper surface, weak shock waves form in proximity of the trailing edge, increase in strength, and coalesce into a single shock wave that moves towards the midchord. As the shock approaches midchord, it weakens appreciably, and the cycle repeats itself periodically with a frequency of 186 Hertz. A similar situation occurs on the lower surface 180 deg. out of phase.

Previous calculations have been performed employing algebraic turbulence models [2],[10],[11],[12]. All the computations reproduced the unsteady features of the flow, but the reduced frequency of oscillations was low by about 20-percent than in the experiments, and the predicted shock wave was more normal, causing the pressure downstream of the shock wave be too high, in some cases double the experimental values. The computations using turbulence models developed for steady flows, even if are able to reproduce the major features of this unsteady flow, do not take into account adequately for turbulence production and destruction mechanism with an appropriate lag to turbulence adjustment to the strong pressure fluctuactions. In [2] and [10], some attempts have been made for taking into account for the lag in adjustment of the turbulence to the changing conditions imposed by the shock wave. The algebraic mixing length model is applied outside the region bounded by the dividing streamline that separates the main and the recirculating regions of the flow. Inside the recirculating region, where the eddy viscosity is varied linearly between the value at the dividing streamline and zero at the airfoil surface, the mixing length is frozen at the value achieved prior the separation.

Moreover all the algebraic turbulence model computations predict a smaller movement of the shock. A better prediction of the reduced frequency is obtained employing the one-equation model of Spalart-Allmaras [1], but the numerical computation does not predict motion of the shock forward of midchord.

In the present work we report the results of the computations obtained with the the two-equation turbulence model (14) and (15).

Governing Equations. The Averaged Navier-Stokes equations (5), (6) and (7), are written in generalized coordinates,

$$\frac{1}{J}\frac{\partial Q}{\partial t} + \frac{\partial \hat{F}}{\partial \xi} + \frac{\partial \hat{G}}{\partial \eta} = \frac{1}{Re}\left(\frac{\partial \hat{F}_v}{\partial \xi} + \frac{\partial \hat{G}_v}{\partial \eta}\right) \quad , \quad (16)$$

where $J = (x_\xi y_\eta - x_\eta y_\xi)^{-1}$ is the Jacobian of the coordinate transformation. Neglecting, for sake of simplicity, the symbols denoting averaged quantities, $Q = (\rho, \rho u, \rho v, E)^T$, is the vector of the conserved variables, and

$$\begin{aligned} \hat{F} &= y_\eta F - x_\eta G \quad , \\ \hat{G} &= -y_\xi F + x_\xi G \quad , \\ \hat{F}_v &= y_\eta F_v - x_\eta G_v \quad , \\ \hat{G}_v &= -y_\xi F_v + x_\xi G_v \quad . \end{aligned}$$

The convective fluxes F and G are defined as follows

$$F = \begin{pmatrix} \rho u \\ \rho u^2 + p \\ \rho uv \\ (\rho E + p)u \end{pmatrix} \quad , \quad G = \begin{pmatrix} \rho v \\ \rho uv \\ \rho v^2 + p \\ (\rho E + p)v \end{pmatrix} \quad ;$$

and the viscous fluxes F_v and G_v

$$F_v = \begin{pmatrix} 0 \\ \tau_{\xi\xi} \\ \tau_{\xi\eta} \\ u\tau_{\xi\xi} + v\tau_{\xi\eta} + q_\xi \end{pmatrix} \quad ,$$

$$G_v = \begin{pmatrix} 0 \\ \tau_{\xi\eta} \\ \tau_{\eta\eta} \\ u\tau_{\xi\eta} + v\tau_{\eta\eta} + q_\eta \end{pmatrix} \quad ;$$

where $\tau_{\xi\xi}$, $\tau_{\xi\eta}$ and $\tau_{\eta\eta}$ denote the transformed total, viscous and inviscid, stresses, and q_ξ and q_η the total heat fluxes.

The spatial derivatives are discretized with second-order accurate central differences, and second-order and fourth-order artificial dissipation terms are added to maintain numerical stability. The equations are solved implicitly in time with an approximate-factorization method and Newton linearization.

Writing equation (16) in the form

$$\frac{1}{J}\frac{\partial Q}{\partial t} = L(Q) \quad ,$$

the linear multistep time integration scheme is

$$(1+\phi)\,Q^{n+1} - (1+2\phi)\,Q^{n} = \qquad (17)$$
$$J\Delta t\left[\theta\mathcal{L}(Q^{n+1}) + (1-\theta)\mathcal{L}(Q^{n})\right] \quad ,$$

with $\phi = 0.5$ and $\theta = 1.$, second order accuracy in time is obtained.

To avoid inversion of block-pentadiagonal matrices, the Jacobians of the fluxes, resulting from the Newton linearization, are diagonalized as suggested in [13], and the left and right eigenvector matrices are carried outside of the spatial derivative operators. The algorithm then requires two scalar pentadiagonal inversions, plus three matrix-vector multiplications, with a substantial saving in computing time and memory requirements. Because of the method with which the left-hand side is treated, second-order accuracy is not attained. To recover second-order accuracy in time, a subiteration strategy based on the pseudo time τ is performed at each time step [14], by replacing relation (17) with

$$\delta Q + \Delta\tau\left[\delta\dot{Q} + \left(\frac{\partial\mathcal{L}}{\partial Q}\right)\delta Q\right] = \qquad (18)$$
$$= \Delta\tau\left[\dot{Q} + J\left(\theta\mathcal{L}(Q^{k}) + (1-\theta)\mathcal{L}(Q^{n})\right)\right] \quad ,$$

with $\delta Q = Q^{k+1} - Q^{k}$, $\delta\dot{Q} = \dot{Q}^{k} - \dot{Q}^{k-1}$ and

$$\dot{Q}^{k} = (1+\phi)\,\frac{Q^{k} - Q^{n}}{\Delta t} - \phi\frac{Q^{n} - Q^{n-1}}{\Delta t} \quad .$$

Results. The computations about the 18-percent thick circular-arc airfoil, with chord $L = 0.203$ meters, $M_\infty = 0.76$ and a chord-based Reynolds number of 11×10^{6}, have been performed on a 291×79 C mesh, with 199 points on the airfoil, the grid points are stretched towards the airfoil. Boundary conditions are no-slip condition and adiabatic temperature on the airfoil. At the inlet boundary free-stream conditions are specified, while characteristic boundary conditions are imposed at the outlet.

In Figure 1, we report the lift coefficient variation as a function of the nondimensional time $t/\left(L/U_\infty\right)$. The oscillatory behavior corresponds to a reduced frequency of 0.43, which is 10-percent lower than the experimental value 0.49 [9].

In Figure 2, the time variation of the nondimensional shock position x_{sh}/L is compared with the measured shock location [9]. It is interesting to note that the present model is able to represent the shock movement also for $x/L < 0.5$, while

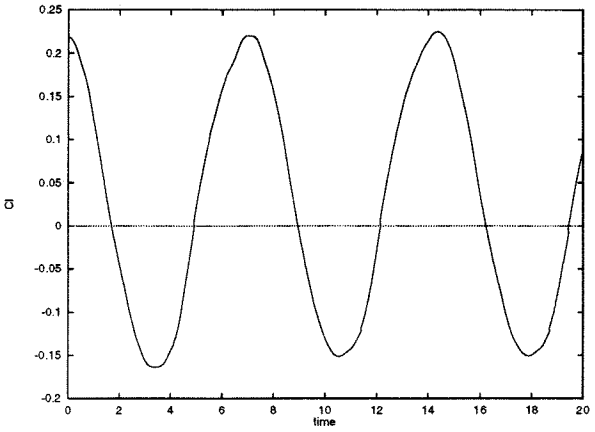

Figure 1: Lift coefficient time variation

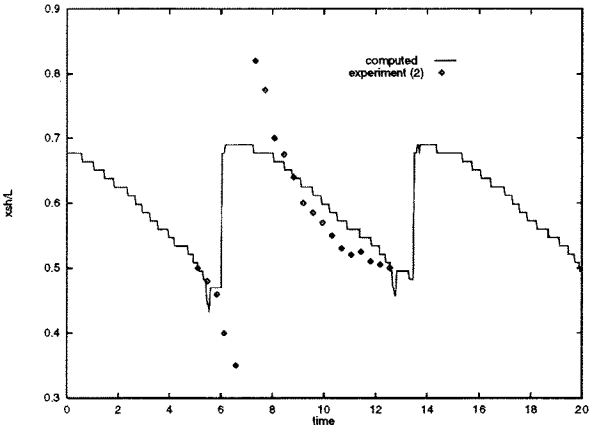

Figure 2: Shock position time variation

other models failed to predict the motion of the shock forward of midchord.

Upper surface pressure coefficient distributions taken at different times during the unsteady cycles, are shown in Figure 3. They agree with the numerical results obtained in [1], using the Spalart-Allmaras turbulence model.

Finally in Figures 4-1/8, the unsteady Mach contours plots, for the same nondimensional times of Figure 3 are shown.

Conclusions

The averaged Navier-Stokes equations and the $k-\varepsilon$ turbulence model, written in the pointwise formulation $k - \mathcal{R}$, have been employed for the prediction of the unsteady flow on a 18-percent thick circular-arc airfoil in supercritical regime. The computed reduced frequency of oscillations is 10-percent lower than the experimental value. The motion of the shock is well represented, and part of the motion forward the midchord is predicted.

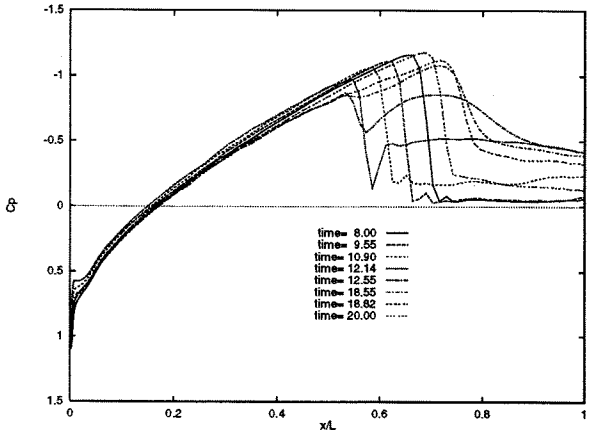

Figure 3: Upper surface pressure coefficient

The two-equation model is able to take into account the lag in response of the turbulence to the sudden changes imposed by the moving shock wave. However further investigations are necessary for assessing the real ability of two-equation turbulence models to capture all the features of the unsteady flow field, by comparing the velocity profiles, as well as the turbulence kinetic energy and Reynolds stress profiles, with the experimental measurements.

References

(1) Rumsey, C. L. et al., "Efficiency and Accuracy of Time-Accurate Turbulent Navier-Stokes Computations", AIAA-95-1835-CP, June 1995.

(2) Seegmiller, H.L., Marvin, J.G. and Levy Jr., L.L., "Steady and Unsteady Transonic Flow", *AIAA Journal*, vol. 16, 1978, pp. 1262-1270.

(3) Reynolds, W.C. and Hussain, A.K.M.F., "The Mechanics of an Organized Wave in Turbulent Shear Flow. Part 3. Theoretical Models and Comparisons with Experiments", *Journal of Fluid Mechanics*, vol. 54, part 2, 1972, pp. 263-288.

(4) Cantwell, B. and Coles, D., "An Experimental Study of Entrainment and Transport in the Turbulent Near Wake ofa CIrcular Cylinder", *Journal of Fluid Mechanics*, vol. 136, 1983, pp. 321-374.

(5) Germano, M., "Turbulence: the filtering approach", *Journal of Fluid Mechanics*, vol. 238, 1992, pp. 325.

(6) Launder, B.E. and Sharma, B.I., "Application of the Energy-Dissipation Model of Turbulence to the Calculation of Flow Near a Spinning Disc", *Heat and Mass Transfer*, Vol. 1, 1974, pp. 131-138.

(7) Chien, K., "Predictions of Channel and Boundary-Layer Flows with a Low-Reynolds Number Turbulence Model", *AIAA Journal*, vol. 20, Jan. 1982, pp. 33-38.

(8) Baldwin, B.S. and Barth, T.J., "A One-Equation Turbulence Transport Model for High Reynolds Number Wall-Bounded Flows", NASA TM-102847, August 1990.

(9) McDevitt, J.B., "Supercritical Flow About a Thick Circular-Arc Airfoil", NASA TM-78549, January 1979.

(10) Marvin, J.G., Levy Jr., J.J and Seegmiller, H.L., "Turbulence Modeling for Unsteady Transonic Flows",*AIAA Journal*, vol. 18, May 1980, pp. 489-496.

(11) Steger, J., "Implicit Finite-Difference Simulation of Flow About Arbitrary Two-Dimensional Geometris", *AIAA Journal*, vol. 16, July 1978, pp. 679-686.

(12) Edwards,J. and Thomas, J., "Computational Methods for Unsteady Transonic Flows", *Unsteady Transonic Aerodynamics, AIAA Progress in Astronautics and Aeronautics*, Nixon, D. (ed.), Vol. 120, Washington, D.C., 1989, pp. 211-261.

(13) Pulliam, T., "Time Accuracy and the Use of Implicit Methods", AIAA 93-3360-CP, July 1993.

(14) Ceresola, N., Alenia Internal Report, 1996.

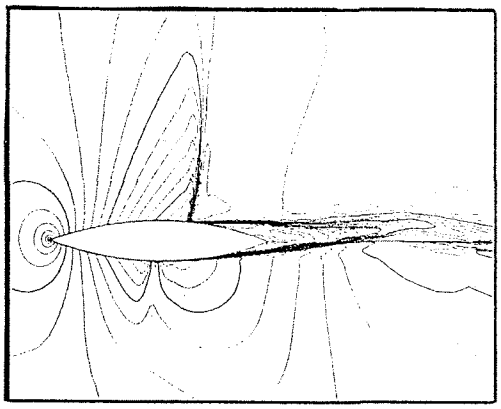

fig. 4.1: Mach Contours, time=8.0, C_L=0.155

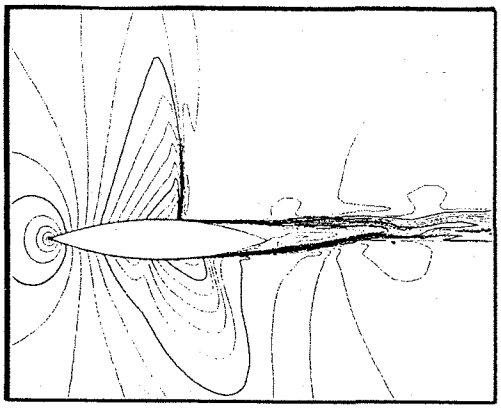

fig. 4.2: Mach Contours, time=9.55, C_L=-0.09

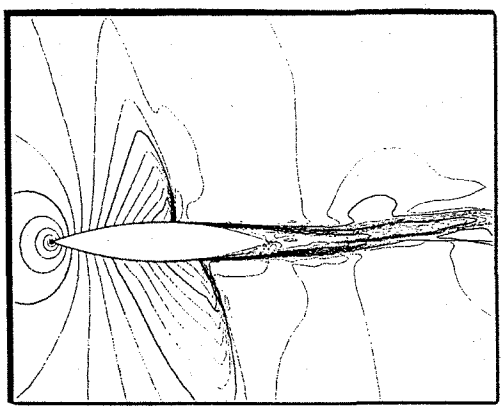

fig. 4.3: Mach Contours, time=10.90, C_L=-0.138

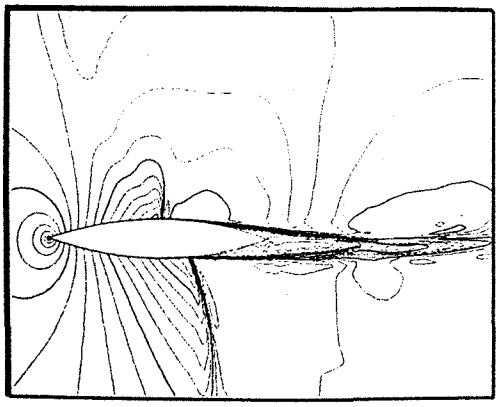

fig. 4.4: Mach Contours, time=12.14, C_L=0.008

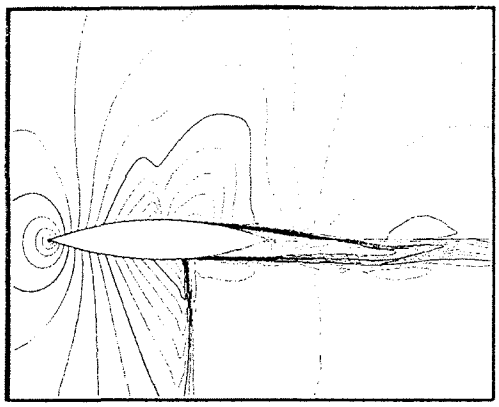

fig. 4.5: Mach Contours, time=12.55, C_L=0.008

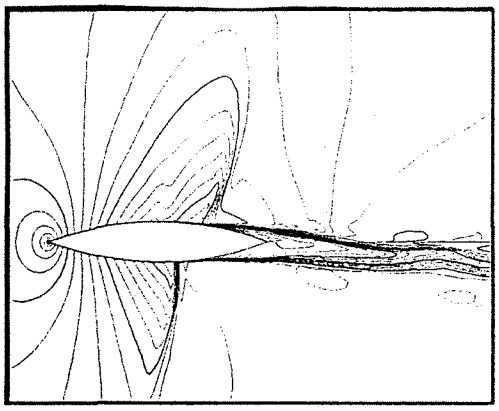

fig. 4.6: Mach Contours, time=18.55, C_L=0.160

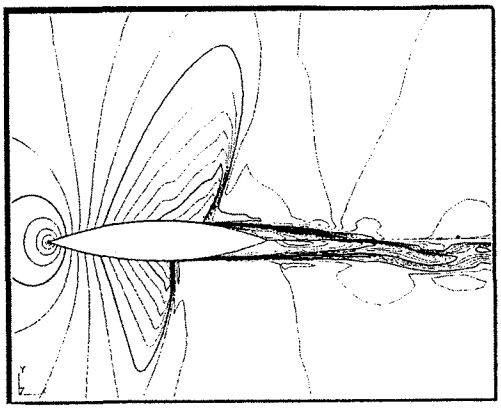

fig. 4.7: Mach Contours, time=18.82, C_L=0.180

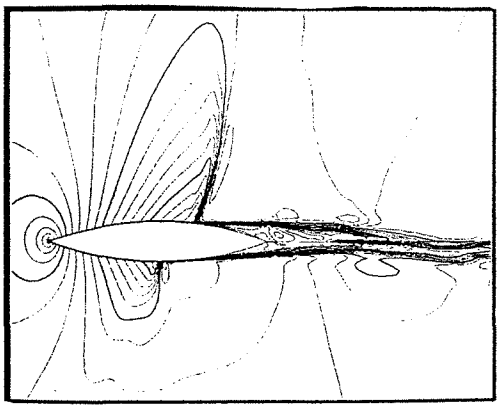

fig. 4.8: Mach Contours, time=20.0, C_L=0.148